Growth and structural characterization of strained epitaxial $Hf_{0.5}Zr_{0.5}O_2$ thin films

Luis Torrejón,[1] Eric Langenberg,[2,3] César Magén,[2,3,4] Ángel Larrea,[2] Javier Blasco,[2,3] José Santiso,[5]
Pedro A. Algarabel[2,3] and José A. Pardo[1,4,6,*]

[1]*Instituto de Nanociencia de Aragón, Universidad de Zaragoza, 50018 Zaragoza, Spain*
[2]*Instituto de Ciencia de Materiales de Aragón, Universidad de Zaragoza – CSIC, 50009 Zaragoza, Spain*
[3]*Departamento de Física de la Materia Condensada, Universidad de Zaragoza, 50009 Zaragoza, Spain*
[4]*Laboratorio de Microscopías Avanzadas, Instituto de Nanociencia de Aragón, Universidad de Zaragoza, 50018 Zaragoza, Spain*
[5]*Catalan Institute of Nanoscience and Nanotechnology (ICN2), CSIC, Barcelona Institute of Science and Technology,*
Campus UAB, Bellaterra, Barcelona, Spain
[6]*Departamento de Ciencia y Tecnología de Materiales y Fluidos, Universidad de Zaragoza, 50018 Zaragoza, Spain*

Ferroelectricity was recently reported in thin films with several compositions in the HfO_2-ZrO_2 system with orthorhombic crystal structure. In the present paper we study the growth by pulsed laser deposition and the structural characterization of strained epitaxial $Hf_{0.5}Zr_{0.5}O_2$ films on (001)-oriented yttria-stabilized zirconia (YSZ) substrates. We have determined the conditions for the coherent growth and correlated the deposition parameters with the films structure and microstructure studied through a combination of x-ray diffraction, electron backscatter diffraction, and scanning transmission electron microscopy. In the range of experimental parameters explored, all the films show monoclinic structure with distorted lattice parameters relative to bulk.

I. INTRODUCTION

Ferroelectric materials present a broad range of technological applications: capacitors, piezoelectric transducers, pyroelectric detectors, ferroelectric random access memories, magnetic field sensors, etc. [1]. Some of the most widely used ferroelectrics are relatively complex oxides, such as $(Ba,Sr)TiO_3$, $Pb(Zr,Ti)O_3$, and $SrBi_2Ta_2O_9$. Consequently, the recent discovery of ferroelectricity in simple oxides of the IV-group transition metals has triggered an intense research activity on this family of compounds. After the initial report on ferroelectric Si-doped HfO_2 films [2], ferroelectricity or antiferroelectricity was observed or predicted in thin films of undoped HfO_2 (Refs. [3,4]) and ZrO_2 (Refs. [5,6]), $Hf_{1-x}Zr_xO_2$ solid solutions [7,8], and ZrO_2/HfO_2 multilayers [9,10], as well as in the modified oxides with several dopants [11,12]. A ferroelectriclike behavior was claimed even in ultrathin TiO_2 films [13]. From the basic point of view, the attempts to clarify the novel mechanisms underlying the unexpected ferroelectricity of such simple compounds are still underway. Furthermore, this phenomenon will have important practical implications, as HfO_2 is largely used in the microelectronics industry due to its compatibility with silicon, high dielectric constant, wide band gap, large breakdown field, and superior thermal and chemical stability [14]. Specific applications of ferroelectric HfO_2-based materials for supercapacitors, memories, field-effect transistors, pyroelectric infrared sensors, cooling devices, or microelectromechanical systems have been explored and are reviewed in a number of publications [15–18].

HfO_2 and ZrO_2 are very similar in their structure and properties and show total solubility in the whole compositional range [19]. In thermodynamic equilibrium at ambient pressure, the $Hf_{1-x}Zr_xO_2$ solid solution (hereafter denoted HZO) presents for any x value a high-temperature fluorite-type cubic structure which transforms upon cooling into a tetragonal one, and then to the room-temperature stable monoclinic phase through a martensitic transformation involving a large volume expansion. However, several metastable phases with orthorhombic symmetry were prepared in this system by high-pressure synthesis [20–22]. Of particular interest is the early report of a noncentrosymmetric orthorhombic phase in Mg-doped ZrO_2 (Ref. [23]).

The delicate energy balance between the structural variants of the HZO system is likely to induce transitions between them driven by small external perturbations, such as mechanical stress or chemical doping [24–26]. In the case of the recently reported HZO thin films, the dependence of the ferroelectric behavior on the film thickness and grain size, substrate, bottom electrode, capping layer, thermal treatment, dopants, or electric-field cycling, has been analyzed [11,27]. However, most of the studies published to date on ferroelectric HZO refer to polycrystalline films with grain dimensions in the nanometer range. The large surface-to-volume ratio of these nanometer-sized grains, together with the strain imposed by the substrate, have been proposed as the driving forces allowing the stabilization of the nonequilibrium structure [3,7,28]. This phase belongs to the orthorhombic space group $Pbc2_1$ and its lack of inversion symmetry is now believed to be at the origin of the ferroelectric behavior of HZO [29]. Nevertheless, the possible influence of grain boundaries, oxygen vacancies, impurities, and other defects on the stabilization of this orthorhombic phase and its ferroelectric behavior has not been

*Corresponding author: jpardo@unizar.es

sufficiently studied. To overcome these limitations, single-crystal and epitaxial films of the pure oxides would be the ideal playground to disentangle intrinsic and extrinsic effects. In this sense, the reports on the preparation and electrical characterization of epitaxial films are very scarce and limited to yttrium-doped HfO_2 films, where the 3+ oxidation state of Y induces the presence of oxygen vacancies [30].

In addition to the experimentally observed phases of HZO and the corresponding terminal compounds, density-functional theory (DFT) calculations have predicted the occurrence of several other structures under the appropriate conditions of pressure, temperature, or applied electric fields [31,32]. Orthorhombic, monoclinic, and triclinic phases lacking inversion symmetry, and thus compatible with ferroelectricity, could in principle be stabilized through epitaxial growth as a result of the biaxial distortion exerted by the substrate [26,31,32]. According to these DFT predictions [31], the $Pbc2_1$ orthorhombic structure can be grown by compressing the $P4_2/nmc$ parent phase along one of the orthorhombic axes, thus inhibiting the transition from the tetragonal to the larger-volume, stable monoclinic $P2_1/c$ structure. In fact, the growth of coherently strained epitaxial films on the appropriate substrates is a well-known strategy used to prepare metastable phases of oxides through the so-called epitaxial stabilization [33]. In the particular case of thin films of ferroelectric oxides, this technique allows engineering their functional properties by tuning the epitaxial strain value [34] and even inducing ferroelectricity in nonferroelectric materials [35,36].

Our goal in the present study is, hence, to prepare strained HZO epitaxial films, determine their structure resulting from epitaxial strain and correlate their microstructure and functional properties with the deposition conditions. We focus on the 50% ZrO_2-50% HfO_2 solid solution, as polycrystalline films with this composition show robust ferroelectricity down to few nanometers thickness, with significant remanent polarization and piezoelectric response [7,27,37].

II. EXPERIMENTAL

A ceramic target with composition $Hf_{0.5}Zr_{0.5}O_2$ was prepared by solid-state reaction. Stoichiometric amounts of HfO_2 and ZrO_2 were mixed, ground, and calcined at 1000 °C overnight. Then, the powder was ground, pressed, and sintered at 1400 °C for 3 days in air. The resulting crystal structure was analyzed by x-ray diffraction (XRD) in a Rigaku D/max-B instrument with a copper rotating anode and a graphite monochromator to select the Cu-$K\alpha$ radiation. The step-scanned patterns of the sample revealed a monoclinic single phase. The crystal structure of the $Hf_{0.5}Zr_{0.5}O_2$ polycrystalline target resolved by x-ray powder diffraction and Rietveld refinement confirmed the expected monoclinic structure (space group $P2_1/c$, No. 14) with lattice parameters $a = 5.1348(3)$ Å, $b = 5.1920(3)$ Å, $c = 5.3078(3)$ Å, $\beta = 99.196(3)°$, and cell volume $V = 139.69(1)$ Å^3.

The $Hf_{0.5}Zr_{0.5}O_2$ films were grown by pulsed laser deposition (PLD) on (001)-oriented yttria-stabilized zirconia (YSZ) substrates, with a cubic fluorite structure (lattice constant 5.15 Å), similar to all the forms of HZO and exerting compressive stress on its longest axes [21,24,26]. We used a

commercial chamber from Neocera with background pressure below 10^{-7} Torr and a KrF excimer laser with 248 nm wavelength. The laser repetition rate was kept at 10 Hz and the fluence on the target at around 1 J/cm^2. The substrate temperature and oxygen pressure in the chamber during growth were systematically scanned in the ranges 250 °C–850 °C and 10^{-4}–10^{-1} Torr, respectively. For selected values of the substrate temperature, films with 5, 10, 15, 30, 80, and 90 nm thicknesses were deposited.

The crystal structure and thickness of the films were studied by XRD and x-ray reflectometry (XRR) using a Bruker D8 Advance high-resolution diffractometer equipped with parallel-beam optics and monochromatic Cu-$K\alpha_1$ radiation (1.54056 Å wavelength). Reciprocal space maps of several HZO structures were simulated by the Wizard software from Bruker. The Hf/Zr ratio in the films was measured by x-ray photoelectron spectroscopy (XPS) in a Kratos Axis SUPRA spectrometer employing a monochromatic Al Kα (1486.6 eV) x-ray source. The spectra were analyzed using Casa software, including background subtraction of a Shirley baseline. The local microstructure was observed by scanning transmission electron microscopy (STEM) on a probe corrected FEI Titan 60–300 microscope equipped with a high-brightness field emission gun (X-FEG) and a CEOS aberration corrector for the condenser system. This microscope was operated at 300 kV to enable a probe size below 1 Å. In order to explore the presence of twin domains and measure their size and crystallographic orientation, electron backscatter diffraction (EBSD) was carried out using an HKL detection system from Oxford Instruments installed in a Merlin (Carl Zeiss) field emission scanning electron microscope (SEM). The electron probe had 15–20 kV energy, depending on the film thickness, and 1 nA current. Charge was compensated using the gas injection system of the SEM [38]. Energy-dispersive x-ray spectroscopy (EDS) was used to verify the lateral homogeneity of the elemental composition of the films.

III. RESULTS AND DISCUSSION

In the search for the optimal growth conditions of epitaxial HZO films, we carried out first a systematic study of the effect of the substrate temperature during deposition on the films structure. The expected 50% Hf–50% Zr concentration was confirmed in these samples by XPS and the lateral homogeneity of the Hf and Zr distribution was proved by EDS. Figure 1 shows the symmetric $\theta/2\theta$ XRD profiles around the YSZ (002) reflection, measured in 10 nm-thick films grown under 10-mTorr oxygen pressure. The broad rounded peak located around $2\theta \sim 33°$–34° corresponds to the HZO film. No diffraction from the film is observed below a temperature threshold (around 350 °C), pointing out that the thermal energy during growth is insufficient to produce single-crystal samples and they become either amorphous or polycrystalline. For the crystalline films (substrate temperature above 350 °C), no other diffraction peak was detected in the 20°–70° 2θ range, proving the epitaxial growth with a unique out-of-plane interplanar spacing. Von Laue's oscillations can be observed at both sides of the film main reflection, which demonstrate a good crystalline coherence along the whole film thickness. The crystal quality of the films was evaluated by measuring
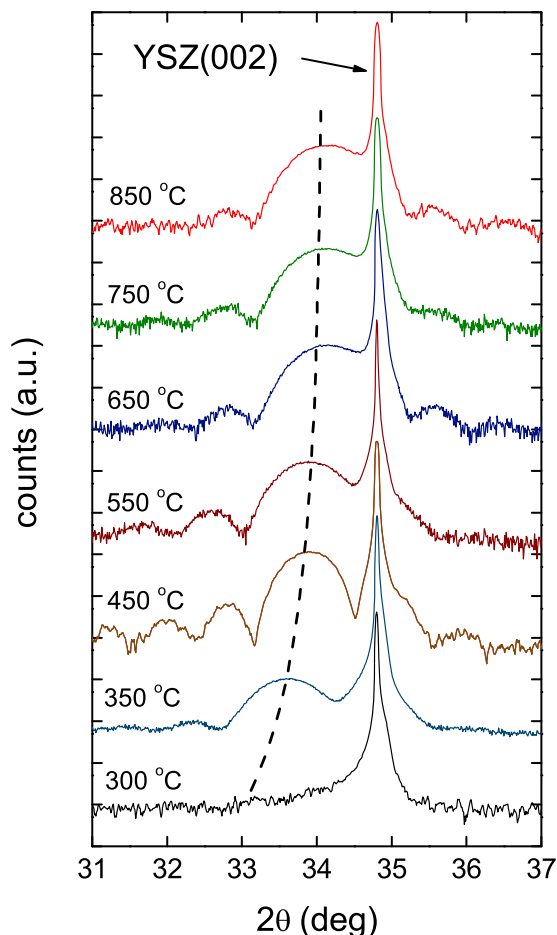
FIG. 1. Symmetric $\theta/2\theta$ XRD patterns around the YSZ (002) reflection, measured in 10-nm-thick HZO films grown at 10 mTorr and different substrate temperatures. The dashed line is a guide to the eye.

rocking curves, i.e., fixing 2θ in Bragg condition and then tilting the incidence angle. These curves (not shown) become slightly narrower upon increasing the deposition temperature, evidencing the continuous improvement of the film crystal quality, as it is commonly observed in epitaxial growth. For instance, full width at half-maximum (FWHM) values of

0.061° and 0.049° were found in 10-nm-thick films grown at 350 °C and 750 °C, respectively.

Rocking curves were also used to study the influence of oxygen pressure in the chamber during deposition. The formation of oxygen vacancies in these films is unlikely, given the huge resistance of ZrO_2 and HfO_2 to reduction. However, this parameter influences the growth process mainly through the plume expansion dynamics. In our experiments, at every fixed growth temperature, the rocking FWHM increased by around 20% for 1 mTorr and 100 mTorr of oxygen relative to the 10 mTorr value. No other significant effect of the oxygen atmosphere was observed, and consequently 10 mTorr was selected as the standard pressure for the epitaxial growth.

To get a deeper insight into the crystal structure of the films, reciprocal space maps were measured around the (113) reflection of the YSZ substrate. Figure 2(a) shows a representative example, obtained in a 10-nm-thick film grown at 550 °C. The two reflections of the film correspond to 2θ values of 55.76° (lower) and 61.41° (upper). Based on the published structural data for all the phases of ZrO_2 and HfO_2 (Refs. [21,24,25]), these reflections are only compatible with a monoclinic structure and can be indexed as (113) and (11$\bar{3}$), respectively (the corresponding 2θ values in our Rietveld refinement of the polycrystalline target are 55.67° and 61.59°). The fact that all three reflections shown in Fig. 2(a) have the same in-plane component (Q_x) of the scattering vector $\vec{Q}$ indicates that the film is coherently strained and its in-plane lattice parameter matches that of the substrate [39]. To study the possible relaxation of this epitaxial strain, we systematically measured reciprocal space maps around the same reflection for all the epitaxial films grown under different experimental conditions. All the maps obtained present the (113) and (11$\bar{3}$) monoclinic reflections of the HZO film aligned vertically with the (113) of the YSZ substrate. This proves that the films remain fully strained for all the experimental conditions explored, even up to the largest thickness values. As an example, Fig. 2(b) shows the result for a 90-nm film deposited at 750 °C.

From the previous diffraction experiments, we conclude that all our HZO films deposited at temperatures equal to and above 350 °C are epitaxial, show monoclinic structure, and grow coherently with their a and b axes parallel to the in-plane cubic directions of the YSZ substrate. As a result of this mechanical constriction, the HZO films have $a = b = 5.15$ Å and thus
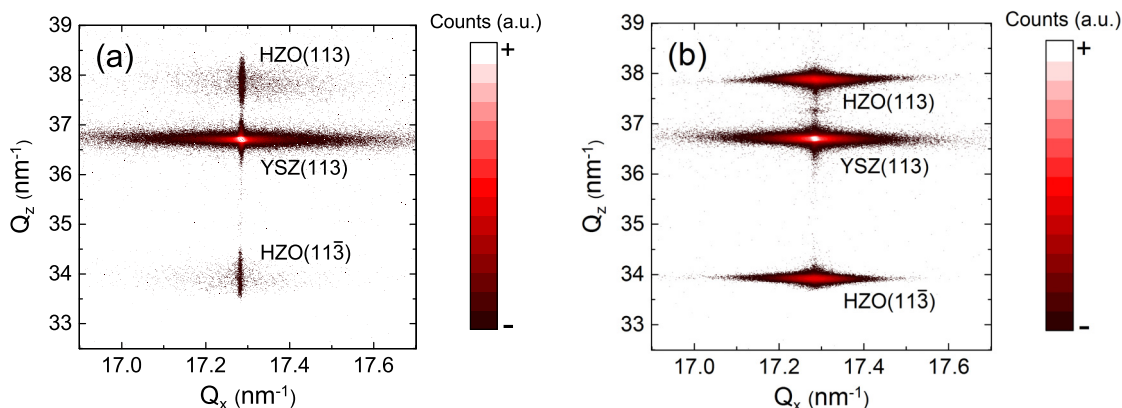

FIG. 2. Reciprocal space maps measured around the YSZ (113) reflection for a 10-nm-thick film grown at 550 °C (a) and for a 90-nm-thick film grown at 750 °C (b).
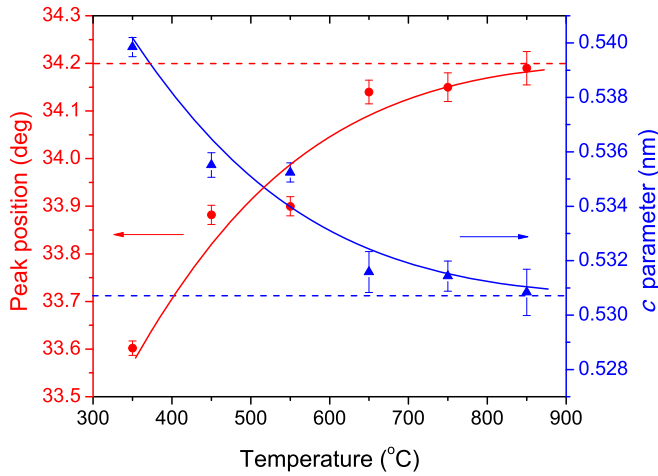
FIG. 3. Dependence of the 2θ angle of the HZO films reflection (left) and the corresponding c lattice parameter (right) with the deposition temperature for the samples shown in Fig. 1. The continuous lines are eye guides and the dashed lines show the respective values of bulk HZO.

distorted lattice parameters and higher symmetry than the bulk phase (which has $a \neq b$). The strain exerted by the substrate on the film along the in-plane directions, defined as the difference between the $Hf_{0.5}Zr_{0.5}O_2$ film and bulk parameters normalized to the latter, results in $+0.3\%$ (tensile) along a and -0.8% (compressive) along b. Regarding the c and β parameters of the film, they can be computed by fitting the $|\vec{Q}_{hkl}|$ values of the monoclinic reflections shown in the reciprocal space maps through the expression

$$\frac{|\vec{Q}_{hkl}|^2}{4\pi^2} = \frac{h^2}{a^2\sin^2\beta} + \frac{k^2}{b^2} + \frac{l^2}{c^2\sin^2\beta} - \frac{2hl\cos\beta}{ac\sin^2\beta}, \quad (1)$$

where $|\vec{Q}_{hkl}|$ is the scattering vector associated with the (hkl) Miller indices [39]. For instance, the fit in the 10-nm film grown at $850\,°C$, the one showing the best crystal quality, yields $a = 5.15\,Å, b = 5.15\,Å, c = 5.31\,Å,\ \beta = 99.15°$, and $V = 139.04\,Å^3$. The monoclinic c axis is thus tilted by $9.15°$ relative to the surface normal and its in-plane projection is parallel to $[100], [010], [\bar{1}00]$, and $[0\bar{1}0]$ directions of YSZ. Essentially, similar results were obtained in the rest of the samples, the β angle being constant within the experimental resolution. In consequence, the film reflection seen in Fig. 1 on the left side of the substrate peak can be indexed as (002) in the monoclinic axes defined previously. Its angular position and the corresponding c parameter depend on the substrate temperature as shown in Fig. 3. It can be seen that c approaches the value of the HZO bulk target as the growth temperature increases.

Although we have proved the epitaxial relation HZO(001)//YSZ(001), given the fourfold rotational symmetry of the substrate along the [001] direction, a tilting of the c axis of the film can take place along the four different YSZ cubic directions on the (001) plane. As a consequence, twin domains with four orientation variants (OV) are expected (see illustration in Fig. 4). The resulting microstructure will have a strong influence on the functional properties of the films. In particular, if they are ferroelectric, the crystallographic
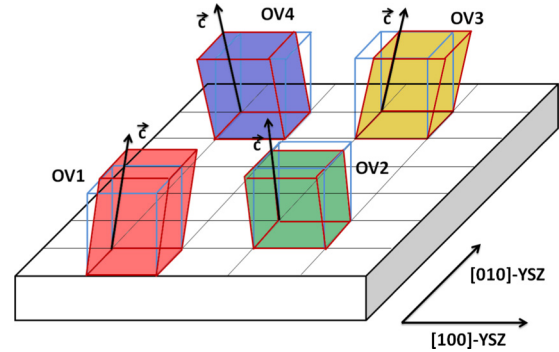

FIG. 4. Schematic illustration showing the possible orientations of twin domains in the monoclinic HZO films grown epitaxially on cubic YSZ.

grain size will fix an upper limit for the ferroelectric domain size. In order to verify these predictions and simultaneously correlate the grain distribution with the deposition conditions, films with different thickness and growth temperature were analyzed using EBSD. Figure 5 shows the EBSD maps of three selected samples [Figs. 5(a)–5(c)], and the ⟨001⟩ pole figure [Fig. 5(d)] for the one presented in Fig. 5(a) (the others are similar). The pole figures show that indeed we do have the four expected orientations. The c axes of the variants are misoriented $9°$ apart from the [001]-YSZ axis and tilted towards the fourfold YSZ symmetry axes, as expected from substrate-film epitaxy relationships. For the EBSD maps we have used a color scheme in which we assigned to each orientation variant a color (red, blue, green, and yellow, in accordance with Fig. 4) corresponding to its orientation in the [001]-HZO pole figure. Just to make it clear, the same color code has been used also for the respective spots in the pole figure represented in Fig. 5(d).

The first conclusion from our EBSD experiments is that the deposition temperature has a strong influence on the size and shape of the grains, as is typically found in thin-film growth [40]. The melting point of HZO with 50% Hf content is $T_m \approx 3100\,K$ (Ref. [19]). In consequence, the films grown at a substrate temperature $T_s = 850\,°C$ (thus $T_s/T_m \approx 0.36$) are in the zone-T regime defined by Petrov *et al.* [41], where surface diffusion is significant. This explains the high degree of faceting and texture visible in Figs. 5(a) and 5(b): the top surface of the grains is approximately triangular in shape, with the sharpest angle pointing towards the in-plane projection of c axis [see pole plot in Fig. 5(d)]. However, at $450\,°C$ $(T_s/T_m \approx 0.23)$ adatom mobilities are quite limited, which gives low lateral growth rates and small domains [Fig. 5(c)]. In fact, in the 30-nm-thick films we have estimated the lateral domain size (D) as the average of square roots of individual surface areas, getting $D \approx 250\,\mu m$ for $T_s = 850\,°C$ [Fig. 5(a)] and $D \approx 5\,\mu m$ for $T_s = 450\,°C$ [smaller grains are shown in Fig. 5(c)].

Figure 5 also shows a marked increase of the monoclinic domain size when the film thickness (t) increases. This is clear by comparing the films grown at $T_s = 850\,°C$, which show lateral domain size $D \approx 0.25\,mm$ for $t = 30\,nm$ [Fig. 5(a)] and $D \approx 0.50\,mm$ for $t = 90\,nm$ [Fig. 5(b)]. At this temperature, competitive growth takes place and grain coarsening occurs due to the coalescence of islands [41]. Three-dimensional
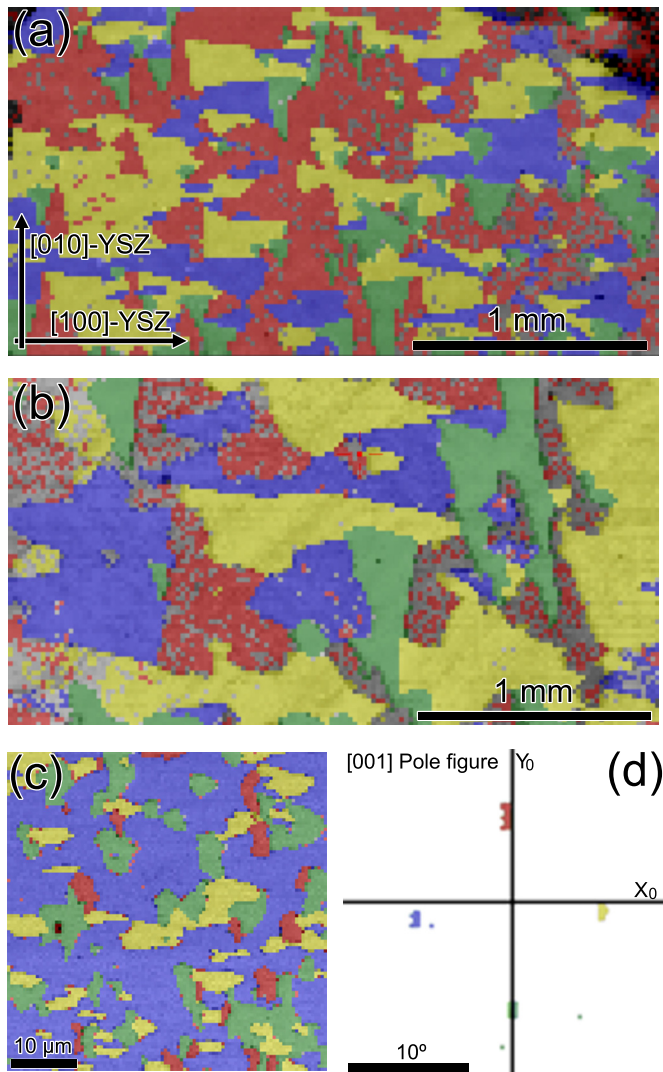
FIG. 5. EBSD maps of the 30-nm-thick HZO film prepared at 850 °C (a), 90-nm-thick HZO film prepared at 850 °C (b), and 30-nm-thick HZO film prepared at 450 °C (c). A zoom of the central part of the $\langle 001 \rangle$-HZO pole figure is shown in (d). The color scheme used for the maps corresponds to the orientation of the different domains in the $\langle 001 \rangle$-HZO pole figure (up: red; right: yellow; left: blue; bottom: green), and is the same as in Fig. 4. The X-Y axes of the three maps and of the pole figure are parallel to the [100] and [010] axes of the YSZ substrate, respectively, as indicated in (a).

simulations of the competition between the vertical growth rates of individual domains in these conditions predicted a $D \sim t^{2/5}$ dependence [42,43]. Although our results contain only two points, $D(t)$ roughly follows a similar trend.

About the relative abundance of the different orientation variants, one could expect, due to the substrate symmetry, that the total area corresponding to each one are similar. In Table I, we collect the area percentage of the four domains on the EBSD maps. For the films prepared at 850 °C the percentages are not dissimilar. The deviation from the theoretically expected value (25%) could be due to incomplete sampling. However, in the case of the film deposited at low temperature [Fig. 5(c)], the majority domain (58%) can almost be considered as a continuous matrix. This unbalance is most probably statistical

TABLE I. Relative occurrence of the four orientation variants estimated from the EBSD experiments.

	Area percentage		
	30 nm–850 °C	90 nm–850 °C	30 nm–450 °C
OV 1	34	26	5
OV 2	15	14	22
OV 3	27	38	15
OV 4	23	22	58

in nature. It must be noted that, for an adequate observation of the domains, the surface scanned in Fig. 5(c) is much smaller (50 μm × 50 μm) than the one of Figs. 5(a) and 5(b) (2.8 mm × 1.5 mm). So a complete scan of the film shown in Fig. 5(c) would produce similar sizes of the different twin domains.

The local structure of individual grains was studied by high angular annular dark field (HAADF) imaging in STEM, a Z-contrast imaging technique useful to image the metal cation lattice. Figure 6(a) shows an atomic resolution cross-section image of a 10-nm-thick HZO film deposited on YSZ at 850 °C, which confirms the growth of an atomically flat epitaxial layer. A detail of this image is highlighted in Fig. 6(b), where the atomic arrangement of the metal cations of the HZO structure can be clearly visualized. Only one kind of structural domain has been observed by STEM analysis. This is perfectly reasonable when taking into account the huge size of the monoclinic domains observed by EBSD (in the range of tens or even a hundred micrometers) in comparison with the sampling area and field of view of STEM, which are typically of 1–2 μm and tens of nanometers, respectively. This crystal structure matches well with the monoclinic phase (space group $P2_1/c$) reported in Ref. [44], with the monoclinic axes b (on the image plane) and a (out of the image plane) in the substrate plane, and the projection of the monoclinic c axis on the image plane and along the growth direction. The HAADF-STEM images confirm that the film grows fully strained by geometrical phase analysis [45] of a lower magnification HAADF image [Fig. 6(c)]. The analysis of the in-plane lattice variation along the image shows that the in-plane lattice parameter of the HZO matches that of the substrate all along the film thickness. No misfit dislocation or strain-relaxing defect is observed. On the other hand, the out-of-plane lattice parameter of the film is 2.6(9)% larger than that of YSZ, which corresponds nicely well with the out-of-plane strain derived from the lattice parameters determined by XRD.

The electrical behavior of the films was assessed through polarization (P) versus field (E) curves measured with the electric field applied along the film plane through patterned interdigital electrodes (results not shown here). The measurements were carried out in representative samples in the temperature range 100 to 300 K and show a linear P-E dependence up to the maximum applied filed ($E = 37.5$ kV/cm). In conclusion, no sign of ferroelectric behavior was detected, as was expected for our HZO films with monoclinic crystal structure. Nevertheless, it is worth reminding that ferroelectric HfO$_2$-based films show unusually high coercive fields, in the order of 1 MV/cm (Refs. [7,11]). This would hinder the detection of hysteretic behavior in our films with this geometry even if they were ferroelectric.
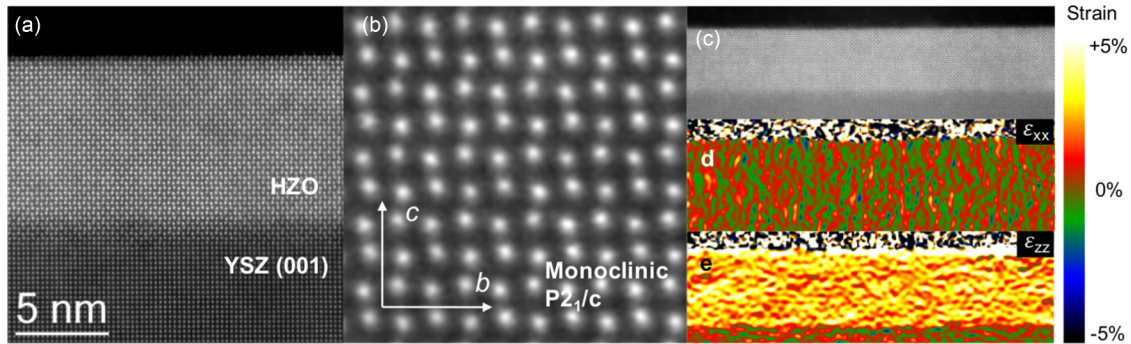
FIG. 6. (a) Aberration corrected HAADF-STEM image of a 10-nm-thick HZO film grown on YSZ (001) at 850 °C. (b) Detail of the atomic structure. (c) Geometrical phase analysis (GPA) of a low magnification image of the same film (top image), including the in-plane deformation (ε_{xx}, central panel), and the out-of-plane deformation (ε_{zz}, lower panel) of the film's lattice parameter with respect to that of the substrate.

Future works aimed at stabilizing one of the orthorhombic phases of HZO through epitaxial strain should probably use higher values of stress. Recent DFT calculations for HfO_2 (Ref. [32]) predict that this could be achieved with a biaxial compression producing an in-plane lattice surface area lower than around $26\,\text{Å}^2$ per unit cell. In the case of our YSZ substrates, this value is $26.5\,\text{Å}^2$. We are currently working to increase the epitaxial strain through the use of different single-crystal substrates.

IV. SUMMARY AND CONCLUSIONS

We have carried out a comprehensive structural and microstructural study by XRD and HRTEM of HZO thin films grown on YSZ (001) substrates by pulsed laser deposition, and determined the optimal conditions for the epitaxial growth of fully coherent monoclinic films. The strains imposed by the cubic substrate on HZO are tensile along a and compressive along b, which gives rise to a distorted monoclinic structure with $a = b$ and thus higher symmetry than the bulk phase. The films present twin domains with four different orientations, as was expected from symmetry considerations and confirmed by EBSD. A strong correlation of the domain size and shape with the film thickness and substrate temperature during deposition has been observed. No ferroelectric behavior was detected in any of the films (within the detection limits). This fact is ascribed to the relatively low epitaxial strain induced by the YSZ substrates on the HZO films, which is not high enough to inhibit the tetragonal to monoclinic transformation. Nevertheless, this study is a preliminary step towards the epitaxial strain-engineered growth of the ferroelectric phases reported or predicted in the HfO_2-ZrO_2 system. Attempts to increase the epitaxial strain through the use of different substrates are underway.

[1] J. F. Scott, Applications of modern ferroelectrics, Science **315**, 954 (2007).

[2] S. Böscke, J. Müller, D. Bräuhaus, U. Schöder, and U. Böttger, Ferroelectricity in hafnium oxide thin films, Appl. Phys. Lett. **99**, 102903 (2011).

[3] P. Polakowski and J. Müller, Ferroelectricity in undoped hafnium oxide, Appl. Phys. Lett. **106**, 232905 (2015).

[4] T. Nishimura, L. Xu, S. Shibayama, T. Yajima, S. Migita, and A. Toriumi, Ferroelectricity of nondoped thin HfO_2 films in TiN/HfO_2/TiN stacks, Jpn. J. Appl. Phys. **55**, 08PB01 (2016).

[5] S. E. Reyes-Lillo, K. F. Garrity, and K. M. Rabe, Antiferroelectricity in thin-film ZrO_2 from first principles, Phys. Rev. B **90**, 140103(R) (2014).

[6] B. Lin, Y. Lu, J. Shieh, and M. Chen, Induction of ferroelectricity in nanoscale ZrO_2 thin films on Pt electrode without post-annealing, J. Eur. Ceram. Soc. **37**, 1135 (2017).

[7] J. Müller, T. S. Böscke, U. Schröder, S. Mueller, D. Bräuhaus, U. Böttger, L. Frey, and T. Mikolajick, Ferroelectricity in simple binary ZrO_2 and HfO_2, Nano Lett. **12**, 4318 (2012).

[8] S. Starschich, T. Schenk, U. Schroeder, and U. Boettger, Ferroelectric and piezoelectric properties of $Hf_{1-x}Zr_xO_2$ and pure ZrO_2 films, Appl. Phys. Lett. **110**, 182905 (2017).

[9] Y. W. Lu, J. Shieh, and F. Y. Tsai, Induction of ferroelectricity in nanoscale ZrO_2/HfO_2 bilayer thin films on Pt/Ti/SiO_2/Si substrates, Acta Mater. **115**, 68 (2016).

[10] S. L. Weeks, A. Pal, V. K. Narasimhan, K. A. Littau, and T. Chiang, Engineering of ferroelectric HfO_2-ZrO_2 nanolaminates, ACS Appl. Mater. Interfaces **9**, 13440 (2017).

[11] M. H. Park, Y. H. Lee, H. J. Kim, Y. J. Kim, T. Moon, K. D. Kim, J. Müller, A. Kersch, U. Schroeder, T. Mikolajick, and C. S. Hwang, Ferroelectricity and antiferroelectricity of doped thin HfO_2-based films, Adv. Mater. **27**, 1811 (2015).

[12] S. Starschich and U. Boettger, An extensive study of the influence of dopants on the ferroelectric properties of HfO_2, J. Mater. Chem. C **5**, 333 (2017).

[13] N. Deepak, M. A. Caro, L. Keeney, M. E. Pemble, and R. W. Whatmore, Interesting evidence for template-induced ferroelectric behavior in ultra-thin titanium dioxide films grown on (110) neodymium gallium oxide substrates, Adv. Funct. Mater. **24**, 2844 (2014).

[14] J. H. Choi, Y. Mao, and J. P. Chang, Development of hafnium based high-k materials—A review, Mater. Sci. Eng. R **72**, 97 (2011).

[15] M. H. Park, H. J. Kim, Y. J. Kim, T. Moon, K. D. Kim, and C. S. Hwang, Thin $Hf_xZr_{1-x}O_2$ films: A new lead-free system for electrostatic supercapacitors with large energy storage density and robust thermal stability, Adv. Energy Mater. **4**, 1400610 (2014).

[16] J. Müller, P. Polakowski, S. Mueller, and T. Mikolajick, Ferroelectric hafnium oxide based materials and devices: Assessment of current status and future prospects, ECS J. Solid State Sci. Technol. **4**, N30 (2015).

[17] M. Hoffmann, U. Schroeder, C Künneth, A. Kersch, S. Starschich, U. Böttger, and T. Mikolajick, Ferroelectric phase transitions in nanoscale HfO_2 films enable giant pyroelectric energy conversion and highly efficient supercapacitors, Nano Energy **18**, 154 (2015).

[18] T. Mittmann, F. P. G. Fengler, C. Richter, M. H. Park, T. Mikolajick, and U. Schroeder, Optimizing process conditions for improved $Hf_{1-x}Zr_xO_2$ ferroelectric capacitor performance, Microelectron. Eng. **178**, 48 (2017).

[19] R. Ruh, H. J. Garrett, R. F. Domagala, and N. M. Tallan, The system zirconia-hafnia, J. Am. Ceram. Soc. **51**, 23 (1968).

[20] R. Suyama, H. Takubo, and S. Kume, Synthesis of $Hf_{1-x}Zr_xO_2$ ($0 < x < 1$) with orthorhombic symmetry, J. Am. Ceram. Soc. **68**, C237 (1985).

[21] E. H. Kisi and C. J. Howard, Crystal structures of zirconia phases and their inter-relation, Key Eng. Mater. **153-154**, 1 (1998).

[22] O. Ohtaka, T. Yamanaka, and S. Kume, Synthesis and x-ray structural analysis by the rietveld method of orthorhombic hafnia, Nippon Seram. Kyo. Gak. **99**, 826 (1991).

[23] E. H. Kisi and C. J. Howard, Crystal structure of orthorhombic zirconia in partially stabilized zirconia, J. Am. Ceram. Soc. **72**, 1757 (1989).

[24] J. E. Lowther, J. K. Dewhurst, J. M. Leger, and J. Haines, Relative stability of ZrO_2 and HfO_2 structural phases, Phys. Rev. B **60**, 14485 (1999).

[25] J. E. Jaffe, R. A. Bachorz, and M. Gutowski, Low-temperature polymorphs of ZrO_2 and HfO_2: A density-functional theory study, Phys. Rev. B **72**, 144107 (2005).

[26] R. Materlik, C. Künneth, and A. Kersch, The origin of ferroelectricity in $Hf_{1-x}Zr_xO_2$: A computational investigation and a surface energy model, J. Appl. Phys. **117**, 134109 (2015).

[27] M. H. Park, H. J. Kim, Y. J. Kim, T. Moon, and C. S. Hwang, The effects of crystallographic orientation and strain of thin $Hf_{0.5}Zr_{0.5}O_2$ film on its ferroelectricity, Appl. Phys. Lett. **104**, 072901 (2014).

[28] R. Batra, H. D. Tran, and R. Ramprasad, Stabilization of metastable phases in hafnia owing to surface energy effects, Appl. Phys. Lett. **108**, 172902 (2016).

[29] X. Sang, E. D. Grimley, T. Schenk, U. Schroeder, and J. M. LeBeau, On the structural origins of ferroelectricity in HfO_2 thin films, Appl. Phys. Lett. **106**, 162905 (2015).

[30] T. Shimizu, K. Katayama, T. Kiguchi, A. Akama, T. J. Konno, O. Sakata, and H. Funakubo, The demonstration of significant ferroelectricity in epitaxial Y-doped HfO_2 film, Sci. Rep. **6**, 32931 (2016).

[31] T. D. Huan, V. Sharma, G. A. Rossetti, and R. Ramprasad, Pathways towards ferroelectricity in hafnia, Phys. Rev. B **90**, 064111 (2014).

[32] R. Batra, T. D. Huan, J. L. Jones, G. Rossetti, and R. Ramprasad, Factors favoring ferroelectricity in hafnia: A first-principles computational study, J. Phys. Chem. C **121**, 4139 (2017).

[33] O. Y. Gorbenko, S. V. Samoilenkov, I. E. Graboy, and A. R. Kaul, Epitaxial stabilization of oxides in thin films, Chem. Mater. **14**, 4026 (2002).

[34] D. G. Schlom, L.-Q. Chen, C. J. Fennie, V. Gopalan, D. A. Muller, X. Pan, R. Ramesh, and R. Uecker, Elastic strain engineering of ferroic Oxides, MRS Bull. **39**, 118 (2014).

[35] D. G. Schlom, L. Q. Chen, C. B. Eom, K. M. Rabe, S. K. Streiffer, and J. M. Triscone, Strain tuning of ferroelectric thin films, Annu. Rev. Mater. Res. **37**, 589 (2007).

[36] C. Becher, L. Maurel, U. Aschauer, M. Lilienblum, C. Magén, D. Meier, E. Langenberg, M. Trassin, J. Blasco, I. P. Krug, P. A. Algarabel, N. A. Spaldin, J. A. Pardo, and M. Fiebig, Strain-induced coupling of electrical polarization and structural defects in $SrMnO_3$ films, Nat. Nanotech. **10**, 661 (2015).

[37] A. Chernikova, M. Kozodaev, A. Markeev, D. Negrov, M. Spiridonov, S. Zarubin, O. Bak, P. Buragohain, H. Lu, E. Suvorova, A. Gruverman, and A. Zenkevich, Ultrathin $Hf_{0.5}Zr_{0.5}O_2$ ferroelectric films on Si, ACS Appl. Mater. Interfaces **8**, 7232 (2016).

[38] S. Serrano-Zabaleta, A. Larrea, H. Stegmann, and C. Waltenberg, Electron backscatter diffraction analysis of non-conductive samples using in-situ charge compensation, Microsc. Anal. **27**, 23 (2013).

[39] M. Birkholz, *Thin Film Analysis by X-Ray Scattering* (Wiley, Weinheim, 2006).

[40] M. Ohring, *Materials Science of Thin Films*, 2nd ed. (Academic Press, San Diego, 2001).

[41] I. Petrov, P. B. Barna, L. Hultman, and J. E. Greene, Microstructural evolution during film growth, J. Vac. Sci. Technol. A **21**, S117 (2003).

[42] A. Van der Drift, Evolutionary selection, A principle governing growth orientation in vapour-deposited layers, Philips Res. Rep. **22**, 267 (1967).

[43] J. M. Thijssen, Simulations of polycrystalline growth in $2 + 1$ dimensions, Phys. Rev. B **51**, 1985 (1995).

[44] T. Kiguchi, S. Nakamura, A. Akama, T. Shiraishi, and T. J. Konno, Solid state epitaxy of $(Hf,Zr)O_2$ thin films with orthorhombic phase, J. Ceram. Soc. Jpn. **124**, 689 (2016).

[45] M. J. Hÿtch, E. Snoeck, and R. Kilaas, Quantitative measurement of displacement and strain fields from HREM micrographs, Ultramicroscopy **74**, 131 (1998).